

# Temperature dependence of the conductivity of graphene on boron nitride

Jürgen Schiefele,<sup>1</sup> Fernando Sols,<sup>1</sup> and Francisco Guinea<sup>2</sup>

<sup>1</sup>*Departamento de Física de Materiales, Universidad Complutense de Madrid, E-28 040, Madrid, Spain*

<sup>2</sup>*Instituto de Ciencia de Materiales de Madrid, CSIC, Cantoblanco, E-28 049, Madrid, Spain*

(Dated: May 1, 2012)

The substrate material of monolayer graphene influences the charge carrier mobility by various mechanisms. At room temperature, the scattering of conduction electrons by phonon modes localized at the substrate surface can severely limit the charge carrier mobility. We here show that for substrates made of the piezoelectric hexagonal boron nitride (hBN), in comparison to the widely used SiO<sub>2</sub>, this mechanism of remote phonon scattering is—at room temperature— weaker by almost an order of magnitude, and causes a resistivity of approximately  $3\Omega$ . This makes hBN an excellent candidate material for future graphene based electronic devices operating at room temperature.

PACS numbers: 72.80.Vp, 77.84.Bw, 72.10.Di

## I. INTRODUCTION

Apart from the great theoretical interest in the electronic properties of graphene<sup>1</sup> spurred by the experimental realization of these one atom thick carbon layers,<sup>2</sup> the new material has been soon recognized as a promising candidate for technological applications.<sup>3</sup> At low temperatures, electrons in free standing (that is, suspended above the substrate) graphene sheets can travel in an essentially ballistic manner, without scattering over distances of the order of a micron.<sup>4</sup> With the carrier density tuned to finite values by an applied gate voltage, the temperature dependence of the resistivity in suspended graphene sheets shows a metallic behavior: at temperatures above 50 K, it increases linearly with temperature. The carrier mobility at room temperature in suspended graphene is severely limited by scattering by out of plane flexural phonons,<sup>5,6</sup> resulting in a resistivity that increases quadratically with the temperature. The effect of flexural phonons on the charge carrier mobility can be eliminated by applying strain or placing graphene on a substrate.<sup>7</sup>

Compared to graphene devices on substrates, suspended graphene samples offer charge carrier mobilities which are higher by a factor of ten, approximately.<sup>8</sup> Likewise, the thermal conductivity of graphene on a substrate can be an order of magnitude lower than that of suspended graphene, due to damping of the flexural phonon modes.<sup>9–11</sup> For technological applications, however, the suspended geometry imposes rather strict limitations on the device architecture. Moreover, free floating graphene is always crumpled,<sup>12</sup> with the corrugations inducing effective fields which in turn influence the charge carriers.<sup>13</sup> While many experiments so far involved graphene samples deposited over SiO<sub>2</sub> or grown over SiC substrates, hexagonal boron nitride (hBN) has developed into a promising candidate as a substrate material for improved graphene based devices.<sup>14,15</sup> hBN is a piezoelectric, large band gap insulator isomorphic to graphite. Boron and nitrogen atoms occupy the inequivalent sublattices in the Bernal structure. The lattice mismatch with graphite is

small (1.7%),<sup>16</sup> and hBN is expected to be free of dangling bonds and surface charge traps.

A number of mechanisms limit the low temperature carrier mobility in graphene.<sup>17–19</sup> At room temperature, interaction with optical surface phonon modes on the interface between graphene and the SiO<sub>2</sub> substrate was found to play an important role.<sup>20</sup> It is this mechanism of remote-phonon scattering from an hBN substrate that we want to consider in the present work. In general, the polar phonon modes on the surface of the substrate (with energies of 50–200 meV) create a long-range electric field, which influences the electrons in the graphene sheet, typically around 4 Å away. The influence of remote phonon scattering on the carrier mobility in two-dimensional electron systems is a well-known phenomenon in semiconductor physics, and was investigated for quantum wells and other heterostructures including metal-oxide-semiconductor field-effect transistors (MOSFETs).<sup>21,22</sup> The effect is more pronounced in graphene due to the much smaller vertical dimension of the devices, as determined by the van der Waals distance. Also, the band gap in semiconductor systems prevents low energy interband transitions, which are present in graphene with the two bands touching at the Dirac point or with the metallic band in the case of doping. For single-layer graphene sheets on substrates of SiC or SiO<sub>2</sub>, surface-phonon scattering has been investigated in Refs. 23–25, employing various methods for calculating the conductivity and describing the screening of the interaction by conduction electrons. In the present paper we calculate the resistivity due to surface phonon scattering for hBN substrates. We show below that the temperature dependence of this mechanism scales with the thermal population of surface phonon modes. While for SiO<sub>2</sub> substrates, the resistivity due to remote phonon scattering is known to be comparable or might surpass that due to graphene intrinsic phonons,<sup>20,26</sup> we show that for hBN, the effect is almost an order of magnitude smaller, resulting in desirable high charge carrier mobilities.



are left with

$$\Sigma_s^i(\mathbf{p}, \omega) = \sum_{\mathbf{k}} \left\{ \frac{N_0^i + 1 - n_F[E_s(k)]}{\hbar(\omega - \mu - \omega_0^i) - E_s(k) + i\eta} + \frac{N_0^i + n_F[E_s(k)]}{\hbar(\omega - \mu + \omega_0^i) - E_s(k) + i\eta} \right\} \mathcal{G}_s(\mathbf{k}) (M_{\mathbf{p}-\mathbf{k}}^i)^2 \quad (6)$$

Here,  $n_F$  denotes the Fermi distribution,  $N_0^i$  the thermal occupation of the phonon, and the appearance of the  $2 \times 2$  matrix  $\mathcal{G}_s$  in the electron Green's function (see Eqn. (A4)) is due to the spinor representation of the electron wavefunction in graphene.

### III. QUASIPARTICLE SCATTERING RATE

The scattering rate can be obtained from Eqn. (6) by multiplying the self energy from the left and right with spinor wavefunctions  $\mathbf{F}_{\pm 1}$  (see Eqn. (A2)) for the ingoing and outcomming electron, respectively, and afterwards taking the imaginary part:

$$\Gamma^i(\omega) = -\frac{1}{2\hbar} \text{Im} \sum_{s=\pm 1} \mathbf{F}_{\text{sgn}[\omega]}^\dagger(\mathbf{p}) \Sigma_s^i(\mathbf{p}, \omega) \mathbf{F}_{\text{sgn}[\omega]}(\mathbf{p}), \quad (7)$$

where the incoming momentum  $\mathbf{p}$  is set on-shell, that is  $\hbar\omega = \pm \hbar v_F |\mathbf{p}| - \mu$ , and  $\text{sgn}[\omega] = \pm 1$  for  $\omega > 0$  ( $\omega < 0$ ), respectively. The imaginary part is obtained via  $\text{Im}[x + i\eta]^{-1} = -\pi\delta(x)$ , which yields the following rates  $\Gamma_{\pm}^i(\omega)$  for emission or absorption of a phonon with frequency  $\omega_0^i$ :

$$\Gamma_+^i(\omega) = \frac{\pi}{2\hbar^2} [N_0 + 1 - n_F(\omega - \omega_0^i)] \times \sum_{\mathbf{k}} M_{\mathbf{p}-\mathbf{k}}^2 \delta(v_F k - |\omega - \omega_0^i|) \begin{cases} f_{-1} & \text{for } 0 \leq \omega < \omega_0^i \\ f_1 & \text{else} \end{cases}, \quad (8a)$$

$$\Gamma_-^i(\omega) = \frac{\pi}{2\hbar^2} [N_0 + n_F(\omega + \omega_0^i)] \times \sum_{\mathbf{k}} M_{\mathbf{p}-\mathbf{k}}^2 \delta(v_F k - |\omega + \omega_0^i|) \begin{cases} f_{-1} & \text{for } -\omega_0^i \leq \omega < 0 \\ f_1 & \text{else} \end{cases}. \quad (8b)$$

The total scattering rate is obtained by summing the absorption and emission rates for scattering from all surface phonons  $i$ . The angular factor

$$f_{\pm 1}(\mathbf{k}, \mathbf{p}) = \frac{1}{2} [1 \pm \cos(\theta_{\mathbf{k}} - \theta_{\mathbf{p}})],$$

in Eqns. (8), where  $\mathbf{k} = k(\cos \theta_{\mathbf{k}}, \sin \theta_{\mathbf{k}})$ , distinguishes between intraband (upper sign) and interband (lower sign) scattering<sup>32</sup>, see Eqn. (A5) and the inset in Fig. 1. Terms describing interband scattering are seen to contribute only in the range  $|\omega| \leq \omega_0^i$ .

Figure 1 shows  $\Gamma(\omega)$  at  $T = 300$  K for intrinsic graphene ( $E_F = 0$ , full line) and extrinsic graphene

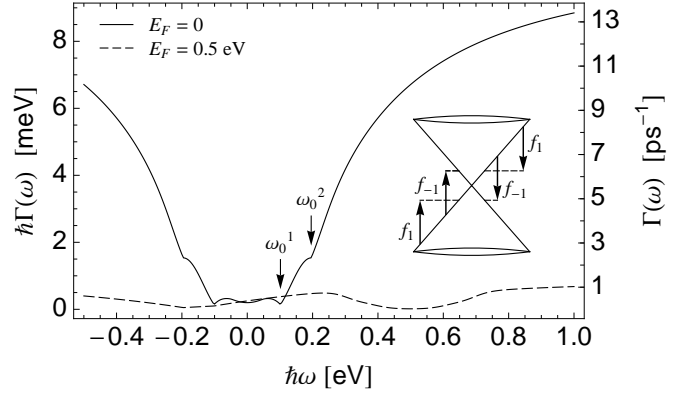


FIG. 1. Quasiparticle scattering rate  $\Gamma(\omega)$  in single layer graphene due to surface phonons of the hBN substrate at  $T = 300$  K [see eqns. (8)]. The frequencies of the optical surface modes  $\omega_0^{1,2}$  are given in table I, the distance between graphene layer and substrate is  $3.40 \text{ \AA}$ . Full line: Intrinsic graphene ( $E_F = 0$ ). Dashed line: Extrinsic graphene with  $E_F = 0.5 \text{ eV}$ . Inset: The angular factor  $f_{\pm 1}$  [see Eqn. (A5)] in the scattering rate distinguishes between interband and intraband scattering.

with  $E_F = 0.5 \text{ eV}$  (corresponding to a carrier density of  $n = 1.83 \cdot 10^{13} \text{ cm}^{-2}$ , dashed line) on a hBN substrate. The distance between graphene layer and substrate is set to  $3.40 \text{ \AA}$ , as found in Ref. 16 for a stacking configuration with one carbon over N, and the other carbon centered above a hBN hexagon<sup>33</sup>. For electron energies around  $E_F \pm \hbar\omega_0^1$ , scattering is strongly suppressed and goes to zero at  $T = 0$ , as there are no empty electronic states below the Fermi energy to scatter into.

The large difference in  $\Gamma$  between the doped and undoped case is due to the Thomas-Fermi screening in Eqn. (3). As this model assumes the instantaneous reaction of the screening charges, our values for  $\Gamma$  at finite doping present a lower bound on the scattering rate.<sup>24,34</sup> If screening is completely neglected, the rate at  $E_F = 0.1 \text{ eV}$  is larger by a factor of four, approximately, which presents an upper bound for the rate.

### IV. SUBSTRATE LIMITED CONDUCTIVITY

We calculate the electrical dc conductivity  $\sigma$  of the graphene layer via the Boltzmann equation:

$$\sigma = \frac{e^2}{h} \int d\omega \frac{|\omega|}{\Gamma_{\text{tr}}(\omega)} \left[ -\frac{dn_F(\omega)}{d\omega} \right] \quad (9)$$

Here, the transport scattering rate  $\Gamma_{\text{tr}}$  is defined as in Eqn. (8), but with an additional factor  $[1 \mp \cos(\theta_{\mathbf{k}} - \theta_{\mathbf{p}})]$  in the integrand (with the upper sign for intraband and the lower one for interband scattering), which lends more weight to large angle scattering events.<sup>30</sup> As the derivative of the Fermi function is sharply peaked around the Fermi energy, the integrand of Eqn. (9) depends mainly on the scattering rate for  $\omega \approx E_F/\hbar$ , where both the

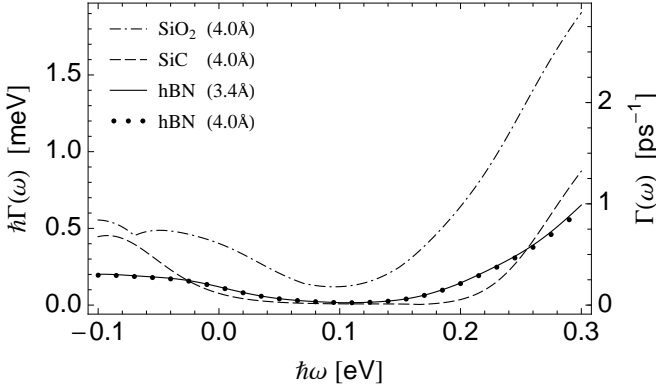


FIG. 2. Scattering rate  $\Gamma(\omega)$  at  $T = 300\text{K}$ ,  $E_F = 0.1\text{ eV}$ , for different substrate materials. The plot shows the energy range around the Fermi energy, which is relevant for the conductivity, for hBN, SiC and SiO<sub>2</sub> substrates. (See table I for the material parameters.) The full line is evaluated with the distance between hBN and graphene set to  $3.4\text{ \AA}$  (see Ref. 16). For comparison, the dots show the rate at a distance of  $4\text{ \AA}$ , as for the other two materials (see Ref. 24). The resulting relative difference in  $\Gamma(E_F)$  is less than 5 per cent.

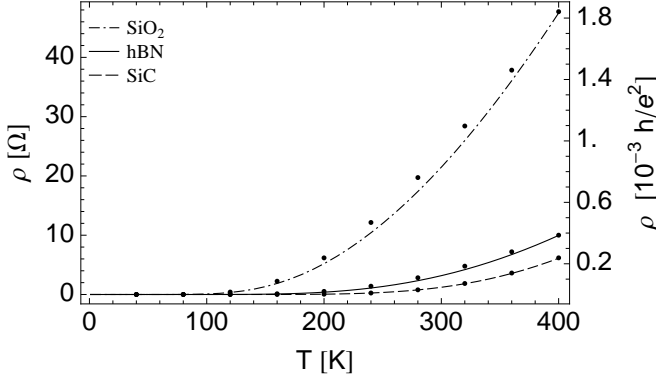


FIG. 3. Temperature dependence of the resistivity for SiO<sub>2</sub>, hBN and SiC (top to bottom). The dots correspond to the population factor  $\rho_0 / \sinh[\hbar\omega_0^1 / (k_B T)]$  (see Eqn. (10)), with  $\rho_0 = 178, 95, 381\text{ }\Omega$  for SiO<sub>2</sub>, hBN, and SiC, respectively.

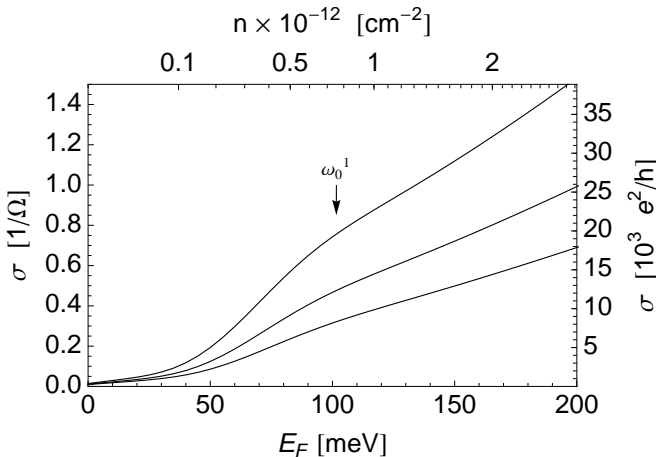


FIG. 4. Conductivity versus Fermi energy for different temperatures  $T = 300, 275, 250\text{ K}$  (bottom to top).

phonon emission and phonon absorption term in Eqn. (8) are proportional to

$$\omega_0^i / \sinh[\hbar\omega_0^i / (k_B T)] . \quad (10)$$

At a given temperature, this is a decaying function of  $\omega_0^i$ . Thus scattering in the relevant range is larger for substrate materials with lower phonon frequencies, which translates into a lower conductivity. In Fig. 2, we compare scattering rates at electron energies near  $E_F = 0.1\text{ eV}$  for different substrate materials. For electrons at the Fermi energy, the rates for SiC and hBN differ roughly by a factor of two, while the scattering rate on SiO<sub>2</sub> is around ten times larger than that on SiC. As the resistivity is calculated from Eqn. (9), its temperature dependence, shown in Fig. 3, is likewise dominated by the population factor (10). We here assume a temperature which is constant throughout the sample, with local heating of the graphene layer prevented by heat dissipation through the substrate.<sup>35</sup>

Regarding the dependence on the charge carrier concentration, the conductivity (9) depends approximately linear on  $E_F$  for energies larger than  $\omega_0^1$  (see Fig. 4). This behaviour is intermediate between that typical for short range scattering,  $\sigma(E_F) \approx \text{const.}$ , and for charged impurity scattering,  $\sigma(E_F) \approx E_F^2$ .<sup>36</sup>

## V. SUMMARY AND CONCLUSIONS

We have analyzed the scattering of graphene electrons from phonons localized at the substrate surface. The temperature dependence of the scattering rate for electrons with energies near  $E_F$  is proportional to the thermal population of these surface phonons, and the same holds for the resistivity. The resistivity induced by the polar surface phonons of hBN substrates at room temperature is of the order of  $3\text{ }\Omega$ , an order of magnitude smaller than the corresponding resistivity of graphene on SiO<sub>2</sub> substrates, in consistency with the higher frequency of these modes in hBN.

For graphene – SiO<sub>2</sub> devices, the temperature dependence of the conductivity was experimentally found to consist of two contributions:<sup>20</sup> scattering by acoustic phonons in graphene and scattering by surface phonons of the substrate. The former shows a linear  $T$  dependence, is independent of the carrier density, and contributes approximately  $30\text{ }\Omega$  at room temperature. The latter is carrier density dependent, follows the bosonic population of the surface modes, and becomes only relevant for  $T > 200\text{ K}$ . At room temperature it is found to dominate the linear term. In experiments with monolayer graphene on hBN,<sup>14</sup> the conductivity shows the same linear temperature dependence as that reported in Ref. 20 for SiO<sub>2</sub>. No indication of activated remote surface phonon scattering was seen up to the experimentally realized temperatures of  $200\text{ K}$ . An estimate of the temperature dependence of the resistivity of graphene on hBN can also be obtained from the experiments reported in Ref. 15. The

result is consistent with the assumption that the room temperature resistivity of graphene on hBN is mainly determined by in plane phonons.

Apart from electron-phonon scattering, Coulomb scattering by charged impurities gives rise to a temperature independent residual resistivity. At carrier concentrations of  $10^{12} \text{ cm}^{-2}$ , this is reported with approximately  $400 \Omega$  for  $\text{SiO}_2$  and roughly three times smaller values for hBN.<sup>14,20</sup>

Our calculation suggests that for graphene on hBN, the temperature-dependent part of the resistivity is –in contrast to  $\text{SiO}_2$  substrates– at room temperature still dominated by electron scattering from the graphene intrinsic phonons, the contribution from interface phonons being negligible. Together with the smaller residual resistivity of graphene on hBN as compared to  $\text{SiO}_2$ , this might allow for graphene – hBN devices with charge carrier mobilities close to that of suspended graphene.

## ACKNOWLEDGMENTS

We are thankful to Andre Geim for providing helpful information. J.S. would like to thank Christopher Gaul and Ivar Zapata for helpful discussions. The authors acknowledge support from the Marie Curie ITN *NanoCTM* and from MICINN (Spain) through Grant No. FIS2010-21372 and FIS2008-00124.

## Appendix A: Matsubara Green's functions and electronic wavefunctions

The Fourier transform of the free thermal Green's function for a surface phonon with frequency  $\omega_0$  is given by

$$D^{(0)}(i\omega_n) = \frac{2\hbar\omega_0}{(i\omega_n)^2 - (\hbar\omega_0)^2}, \quad (\text{A1})$$

where the bosonic Matsubara frequencies are defined as  $\omega_n = 2\pi k_B T n$  with integer  $n$ .<sup>30</sup>

The wavefunction for electronic states in graphene near one of the Dirac points is<sup>1,37</sup>

$$\mathbf{F}_s(\mathbf{r}) = A^{-1/2} \mathbf{F}_s(\mathbf{q}) \exp(i\mathbf{q} \cdot \mathbf{r})$$

where  $s = \pm 1$  denotes the band index,  $A$  is the area of the system and

$$\mathbf{F}_s(\mathbf{q}) = \frac{1}{\sqrt{2}} \begin{pmatrix} e^{-i\theta_{\mathbf{q}}} \\ s \end{pmatrix}. \quad (\text{A2})$$

In the same spinor representation, the electron Green's function is written as the  $2 \times 2$  matrix<sup>38</sup>

$$G_s^{(0)}(\mathbf{k}, i\omega_n) = \mathcal{G}_s(\mathbf{k}) \frac{1}{i\omega_n - E_s(\mathbf{k}) + \mu} \quad (\text{A3})$$

where  $\omega_n = (2n + 1)\pi k_B T$  are the fermionic Matsubara frequencies,  $E_s$  is the energy of the electron (see Eqn. (4)) within the Dirac cone approximation and

$$\mathcal{G}_s(\mathbf{k}) = \frac{1}{2} \begin{pmatrix} 1 & s e^{-i\theta_{\mathbf{k}}} \\ s e^{i\theta_{\mathbf{k}}} & 1 \end{pmatrix}. \quad (\text{A4})$$

The angular factor  $f_{\pm 1}$  appearing in Eqn. (8) is composed of

$$\mathbf{F}_{s'}^\dagger(\mathbf{p}) \mathcal{G}_s(\mathbf{k}) \mathbf{F}_{s'}(\mathbf{p}) = \frac{1}{2} [1 + s s' \cos(\theta_{\mathbf{k}} - \theta_{\mathbf{p}})] \equiv f_{s, s'}(\mathbf{k}, \mathbf{p}). \quad (\text{A5})$$

<sup>1</sup> A. H. Castro Neto, F. Guinea, N. M. R. Peres, K. S. Novoselov, and A. K. Geim, *Rev. Mod. Phys.* **81**, 109 (2009).

<sup>2</sup> K. S. Novoselov, A. K. Geim, S. V. Morozov, D. Jiang, Y. Zhang, S. V. Dubonos, I. V. Grigorieva, and A. A. Firsov, *Science* **306**, 666 (2004).

<sup>3</sup> A. K. Geim and K. S. Novoselov, *Nature Materials* **6**, 183 (2007).

<sup>4</sup> X. Du, I. Skachko, A. Barker, and E. Y. Andrei, *Nature Nano* **3**, 491 (2008).

<sup>5</sup> E. V. Castro, H. Ochoa, M. I. Katsnelson, R. V. Gorbachev, D. C. Elias, K. S. Novoselov, A. K. Geim, and F. Guinea, *Phys. Rev. Lett.* **105**, 266601 (2010).

<sup>6</sup> H. Ochoa, E. V. Castro, M. I. Katsnelson, and F. Guinea, *Phys. Rev. B* **83**, 235416 (2011).

<sup>7</sup> D. L. Nika and A. A. Balandin, *ArXiv e-prints* (2012), 1203.4282.

<sup>8</sup> Y.-W. Tan, Y. Zhang, K. Bolotin, Y. Zhao, S. Adam, E. H. Hwang, S. Das Sarma, H. L. Stormer, and P. Kim, *Phys. Rev. Lett.* **99**, 246803 (2007).

<sup>9</sup> A. A. Balandin, *Nat Mater* **10**, 569 (2011).

<sup>10</sup> L. Lindsay, D. A. Broido, and N. Mingo, *Phys. Rev. B* **82**, 115427 (2010).

<sup>11</sup> Z.-Y. Ong and E. Pop, *Phys. Rev. B* **84**, 075471 (2011).

<sup>12</sup> J. C. Meyer, A. K. Geim, M. I. Katsnelson, K. S. Novoselov, T. J. Booth, and S. Roth, *Nature* **446**, 60 (2007).

<sup>13</sup> M. A. H. Vozmediano, M. I. Katsnelson, and F. Guinea, *Phys. rep.* **496** (2010).

<sup>14</sup> R. C. Dean, A. F. Young, I. Meric, C. Lee, L. Wang, S. Sorgenfrei, K. Watanabe, T. Taniguchi, P. Kim, K. L. Shepard, et al., *Nat Nano* **5**, 722 (2010).

<sup>15</sup> A. S. Mayorov, R. V. Gorbachev, S. V. Morozov, L. Britnell, R. Jalil, L. A. Ponomarenko, P. Blake, K. S.

- Novoselov, K. Watanabe, T. Taniguchi, et al., *Nano Letters* **11**, 2396 (2011).
- <sup>16</sup> G. Giovannetti, P. A. Khomyakov, G. Brocks, P. J. Kelly, and J. van den Brink, *Phys. Rev. B* **76**, 073103 (2007).
  - <sup>17</sup> N. M. R. Peres, *Rev. Mod. Phys.* **82**, 2673 (2010).
  - <sup>18</sup> S. Das Sarma, S. Adam, E. H. Hwang, and E. Rossi, *Rev. Mod. Phys.* **83**, 407 (2011).
  - <sup>19</sup> S. Das Sarma and E. H. Hwang, *Phys. Rev. B* **83**, 121405 (2011).
  - <sup>20</sup> J.-H. Chen, C. Jang, S. Xiao, M. Ishigami, and M. S. Fuhrer, *Nature Nanotechnology* **3**, 206 (2008).
  - <sup>21</sup> M. V. Fischetti, D. A. Neumayer, and E. A. Cartier, *Journal of Applied Physics* **90**, 4587 (2001).
  - <sup>22</sup> N. Mori and T. Ando, *Phys. Rev. B* **40**, 6175 (1989).
  - <sup>23</sup> A. Konar, T. Fang, and D. Jena, *Phys. Rev. B* **82**, 115452 (2010).
  - <sup>24</sup> S. Fratini and F. Guinea, *Phys. Rev. B* **77**, 195415 (2008).
  - <sup>25</sup> X. Li, E. A. Barry, J. M. Zavada, M. B. Nardelli, and K. W. Kim, *Applied Physics Letters* **97**, 232105 (2010).
  - <sup>26</sup> E. H. Hwang and S. Das Sarma, *Phys. Rev. B* **77**, 115449 (2008).
  - <sup>27</sup> S. Q. Wang and G. D. Mahan, *Phys. Rev. B* **6**, 4517 (1972).
  - <sup>28</sup> R. Geick, C. H. Perry, and G. Rupprecht, *Phys. Rev.* **146**, 543 (1966).
  - <sup>29</sup> H. Nienhaus, T. Kampen, and W. Mönch, *Surface Science* **324**, L328 (1995).
  - <sup>30</sup> G. D. Mahan, *Many-particle physics* (Plenum Press, New York, 1981).
  - <sup>31</sup> A. L. Fetter and J. D. Walecka, *Quantum Theory of Many Particle Systems* (Dover Publications, 2003).
  - <sup>32</sup> Eqns. (8) are identical to the result obtained in Ref. 24, while in Refs. 23 and 25, interband scattering is neglected.
  - <sup>33</sup> For other possible stacking configurations, this distance can be around 0.2 Å smaller or larger, see Ref. 16.
  - <sup>34</sup> B. Wunsch, T. Stauber, F. Sols, and F. Guinea, *New Journal of Physics* **8**, 318 (2006).
  - <sup>35</sup> H. Sevinçli, W. Li, N. Mingo, G. Cuniberti, and S. Roche, *Phys. Rev. B* **84**, 205444 (2011).
  - <sup>36</sup> K. Nomura and A. H. MacDonald, *Phys. Rev. Lett.* **98**, 076602 (2007).
  - <sup>37</sup> T. Ando, *Journal of the Physical Society of Japan* **75**, 074716 (2006).
  - <sup>38</sup> T. Stauber and N. M. R. Peres, *Journal of Physics: Condensed Matter* **20**, 055002 (2008).